ARCHIVES OF ELECTRICAL ENGINEERING VOL. X(Y), pp. 1-22 (2026)

This paper has been accepted for publication in the AEE journal. This is the version, which has not been fully edited and content may change prior to final publication.
Citation information: DOI 10.24425/aee.2026.3549

A method for core loss calculation based on sinusoidal losses for DC-DC converters operating at various duty cycle values and temperatures

DAMIAN GZIEŁ, MARIUSZ NAJGEBAUER*

Institute of Electric Power Engineering, Czestochowa University of Technology
al. Armii Krajowej 17, 42-200 Częstochowa, Poland
*e-mail: {damian.gziel/*mariusz.najgebauer}@pcz.pl*

Abstract: The paper presents an experimental verification of a method for computing losses in a magnetic core operating in a DC-DC converter with a variable duty cycle, based on losses measured under sinusoidal excitation conditions. The core operating conditions that influence the losses and the method for their measurement are presented. The measurement setup was designed for this research, its basic features are discussed in the paper. The results obtained from the analysis were compared with core loss measurements obtained from the Brockhaus MPG-200 system. The theoretical foundation for core loss calculations and the measurement error analysis are also presented. The discussion of the results takes into account additional factors, such as the effect of working temperature on loss level.

Key words: DC-DC power converter, magnetic core loss, ferrite, power electronics

1. Introduction

Inductive elements containing magnetic cores are widely used in switching mode power supplies (SMPS). These are very important components that may occupy even 30–50% of the total volume of a power converter [1]. Currently DC-DC power converter modules account for about 35% of the SMPS market [2]. Nowadays there are also strong trends towards increasing the efficiency of power converters, leading to their more compact structure and reduction of energy loss in their magnetic components [3–6] This trend stimulates the engineers' efforts to improve prediction of core losses already at the design stage. For this purpose, a good knowledge of the operating modes of power converters is required. Pulse-width modulation (PWM) is commonly used to control DC-DC power converters [7–10]. When this type of modulation is used, the value of the duty cycle D generated by the control system has a significant impact on the voltage waveform magnetizing the magnetic core operating in a power converter. To maintain a constant DC-DC converter output voltage despite changes in the supply voltage and the load, the control system continuously adjusts the duty cycle D value [11]. The magnetic core operating in a power electronics DC-DC converter, most often in classic solutions using hard switching, is subjected to a rectangular voltage excitation. In the case of isolated converters, the magnetic element transforming the energy is a transformer. In non-isolated systems, it is a inductor, most often acting as an instantaneous energy storage [12]. In more complex DC-DC converter systems, both a transformer and inductors may be used. Depending on the type of magnetic element and the converter topology, an additional constant component of the magnetic field strength (H_{DC}) may be present [13–15]. One of the challenges for power electronics designers, and particularly those who dedicated magnetic components for DC-DC converters, is determination of not only the losses in the magnetic core under specific operating conditions, but also over the entire range of supply and load conditions in which the converter will operate. Loss prediction in a magnetic core is a complex issue, therefore methods based on empirical formulas or provided by the magnetic material manufacturer are popular in engineering practice [16–19]. Core manufacturers typically provide datasheets reporting core loss measurements obtained under standardized measurement conditions that ensure a sinusoidal magnetic flux density in the core [20–21]. This paper experimentally validates the core loss calculation method based on the knowledge of losses under sinusoidal excitation conditions [22–23]. The applicability of the method for a ferrite core operating at a triangular magnetic flux density with different duty cycle values and at different temperatures was investigated.

2. Method description

The example waveform (idealized model case) of the magnetizing voltage and the magnetic flux density in the core is depicted in Fig. 1. Taking into account the duty cycle value $D \neq 0.5$ is possible by decomposing the losses corresponding to the triangular asymmetric magnetic flux density waveform (Fig. 1(a)) into two triangular symmetrical waveforms where $D = 0.5$ (Fig. 1(b)) [23]:

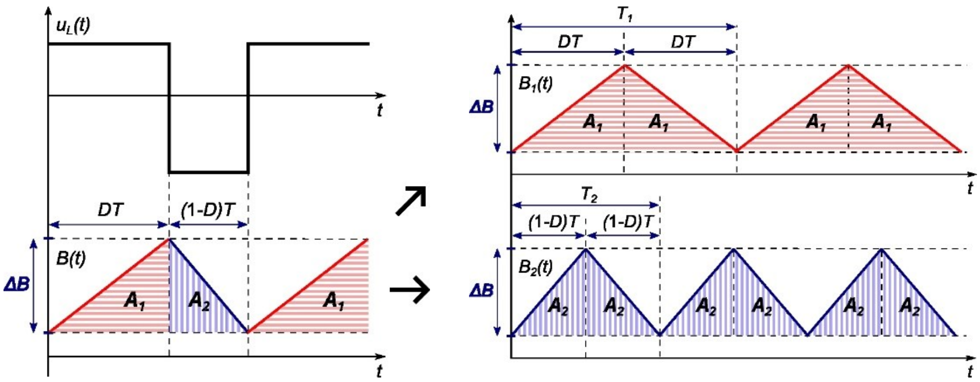

Fig. 1. Square voltage excitation waveform and triangular flux density waveform (under DC bias conditions) (a); corresponding flux density waveforms based on model (b)

This paper has been accepted for publication in the AEE journal. This is the version, which has not been fully edited and content may change prior to final publication.
Citation information: DOI 10.24425/aee.2026.3549

Energy dissipated during one complete rectangular cycle of the magnetizing voltage Q_{rect} in the considered model (which corresponds to the voltage waveform depicted in Fig. 1(a)) is the sum of the lost energies Q_{eq1} and Q_{eq2} (which corresponds to waveforms of the magnetic flux density $B_1(t)$ and $B_2(t)$ depicted in Fig. 1(b)) for the equivalent frequencies f_{eq1} and f_{eq2}, respectively (waveforms depicted in Fig. 2).

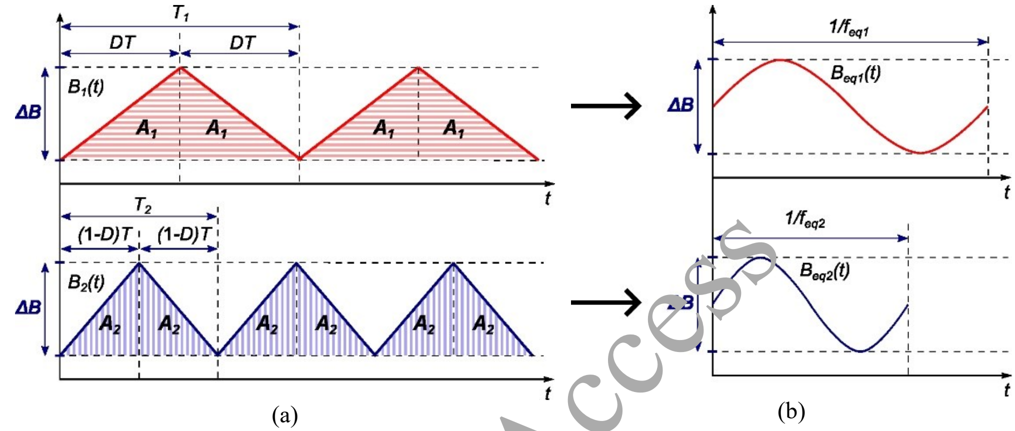

Fig. 2. Corresponding flux density waveforms based on model (a); corresponding equivalent sinusoidal flux density waveform (b)

The energy losses Q_{eq1} and Q_{eq2} ultimately contribute to the losses under the conditions of a rectangular voltage excitation Q_{rect} according to the formula [23]:

$$Q_{\mathrm{rect}}(\Delta B, f_{\mathrm{rect}}, H_{\mathrm{DC}}, \vartheta_s) = \frac{1}{2} Q_{\mathrm{eq1}}(\Delta B, f_{\mathrm{eq1}}, H_{\mathrm{DC}}, \vartheta_s) + \frac{1}{2} Q_{\mathrm{eq2}}(\Delta B, f_{\mathrm{eq2}}, H_{\mathrm{DC}}, \vartheta_s), \qquad (1)$$

where: ΔB is the value of peak-to-peak magnetic flux density (equal to twice the maximum flux density B_m), H_{DC} is the DC component of magnetic field strength, ϑ_s represents the core surface temperature. Formula (1) was tested only for one selected value of the duty cycle of 0.5, while the effect of the core temperature was not previously considered. Thus, the original model presented in [23] has been extended in this study to incorporate the reference temperature of the magnetic core and then validated for various duty cycle values. For its validation, the measured core surface temperature was used as the reference temperature.

Energy losses depend on the derivative of the magnetic flux density $\mathrm{d}B/\mathrm{d}t$. Arbitrary shape of the magnetic flux density can be represented using a linear-segmental description containing a weighting factor. The formula for the equivalent frequency of a sinusoidal signal takes the form [22]:

$$f_{\mathrm{eq}} = \frac{2}{\pi^2} \sum_{k=1}^{K} \left(\frac{B_k - B_{k-1}}{B_{\max} - B_{\min}} \right)^2 \frac{1}{t_k - t_{k-1}}, \qquad (2)$$

This paper has been accepted for publication in the AEE journal. This is the version, which has not been fully edited and content may change prior to final publication.
Citation information: DOI 10.24425/aee.2026.3549

where K is the number of next k-th segments of the linear-segmental magnetic flux density. Applying Formula (2) for the cases presented in Fig. 2, we obtain the following expressions of equivalent frequencies f_{eq1} and f_{eq2}, respectively:

$$f_{\mathrm{eq1}} = \frac{4}{\pi^2 D} f_{\mathrm{rect}}, \quad f_{\mathrm{eq2}} = \frac{4}{\pi^2 D} f_{\mathrm{rect}}, \tag{3}$$

where: f_{rect} is the frequency of the rectangular voltage magnetizing the core (corresponds to the core operating frequency in the DC-DC converter). However, it should be noted that the formulas and waveforms presented in Figs. 1 and 2 contain significant simplifications. In real conditions, the core is not directly magnetized by the voltage supplying the inductor or the transformer primary winding. Due to the losses and leakage inductance occurring in the winding, the core magnetizing voltage is lower than the supply voltage, as it is reduced by the voltage drop across the parasitic elements of the equivalent circuit. The higher the value of the parasitic parameters of equivalent winding resistance and leakage inductance, and the higher the primary winding current, which is more or less distorted depending on the type of core magnetic material, the more distorted the core magnetizing voltage is. The adopted analysis method also ignores the effects of short-term voltage oscillations (a problem described, for example, in [24]) occurring during switching of power electronic converter transistors.

3. Measurement method

Core loss measurements were performed in two stages. The first stage involved measuring core losses under sinusoidal excitation of the magnetic flux density, which corresponds to the right-hand side of Eq. (1). These measurements were carried out using the experimental setup shown in Fig. 3 and a list of the most important equipment is provided in Table 1.

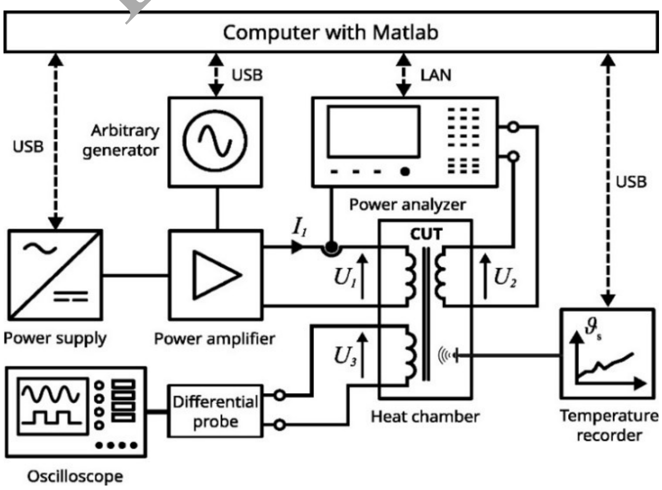

Fig. 3. Experimental measurement setup for equivalent sinusoidal excitation

This paper has been accepted for publication in the AEE journal. This is the version, which has not been fully edited and content may change prior to final publication.
Citation information: DOI 10.24425/aee.2026.3549

Table 1. List of selected equipment included in the measurement setup (from Fig. 3)

Type of device	**Device model**
Power analyzer	Hioki PW-8001
Current probe	Hioki CT6872
Heat chamber	Memmert UN30plus
Temperature recorder	Almemo 710
Infra-red temperature sensor	Almemo FIAD4332
Arbitrary generator	Siglent SDG2042X
Oscilloscope	Tektronix MDO34
Voltage differential probe	Tektronix TMDP0200

The entire measurement process was controlled by a computer using scripts written in the MATLAB environment. The objective of using the self-assembled setup in the first part of the measurements was also to test whether it is possible to replace the specialized equipment for measuring magnetic materials with equipment more frequently used by power electronics engineers. The core under test (CUT) was equipped with two independent measuring windings. All windings, both magnetizing and measuring, had the same number of turns. Measurement of the magnetizing current and the voltage induced in the measuring winding (the induced voltage U_2 shown in Fig. 3) enabled direct determination of the magnetic core losses using the Hioki PW8001 power analyzer. The third winding (the induced voltage U_3 shown in Fig. 3) provided an independent, real-time measurement of the induced voltage. The signal was monitored with an oscilloscope (with only eight-bit resolution) and isolated from the main measurement path. An alternative solution that could be used instead of a power analyzer would be to use only an oscilloscope with sufficiently high bit resolution [25].

The study extended the verification of the method described in [22–23] to include the core surface temperature. Temperature was measured with a FIAD4332 pyrometric sensor connected to an ALMEMO 710 data logger. The pyrometric temperature sensor had a ZR7843CFL focusing lens, which created a measuring field of 1 mm in diameter at a distance of 1 cm from the lens, which contained the tested core surface. In the measuring field, a tape with a known emissivity of $\varepsilon = 0.96$ was glued to the core surface. Due to the dynamics of the measurement process, the measurement control program using the setup presented in Fig. 3 ensured that measurements were made at the set temperature within the maximum assumed range of ±2°C. However, the accuracy of the pyrometric sensor itself was ±1% (or 1°C, whichever is greater). Due to the difficulty of ensuring exactly the same temperature conditions when measuring each of the components Q_{eq1} and Q_{eq2} of Eq. (1) for individual reference temperatures ϑ_{ref}, the measurement results were further processed and modeled in order to finally bring the results to

This paper has been accepted for publication in the AEE journal. This is the version, which has not been fully edited and content may change prior to final publication.
Citation information: DOI 10.24425/aee.2026.3549

the same temperature value along with their uncertainties. It is worth noticing that the measured surface temperature of the magnetic core is not the average temperature of the core itself, nor is it the hottest point within the core structure (hot spot), which also depends on the type of winding [26]. The core internal temperature was not estimated in this research. This complex issue is explained in a simplified and practical manner, among others, in [27]. Since, as indicated by the manufacturer's data [28], the core losses of the N87 ferrite material exhibit a strong dependence on temperature, the entire measurement procedure as well as the treatment of results and uncertainties must account for this fact. A comparison of the measurement results corresponding to both sides of Eq. (1) can only be performed when these results are obtained at identical core temperatures, and therefore when the surface temperature of the core is the same in both cases (assuming that this temperature has stabilized after waiting sufficiently long for the internal structure of the core to reach thermal equilibrium under the same direction of temperature change inside the climatic chamber). For each measurement of magnetic core losses as a function of temperature, the target core surface temperatures were set to the following reference values: 30, 50, 70, 90, 100, 110, and 120°C. A measurement was considered acceptable when the core surface temperature ϑ_s satisfied the condition $\vartheta_s = \vartheta_{\mathrm{ref}} \pm 2$°C. The influence of deviations of ϑ_s from the reference temperature ϑ_{ref} was included in the estimation of the results and uncertainties, as described in the following section.

Since the core losses are represented by the area of the magnetic hysteresis loop *B*-*H*, these can be expressed in reference to the core volume as follows [29]:

$$P_v = \frac{1}{T}\oint H \mathrm{d}B = \int_0^T H \frac{\mathrm{d}B(t)}{\mathrm{d}t}\mathrm{d}t, \tag{4}$$

where: T is the period of the hysteresis loop, which is the inverse of the frequency of the voltage magnetizing the core, H is the magnetic field strength, B is the magnetic flux density. Using Ampere and Faraday laws for the magnetic circuit, the following relations can be used:

$$H(t) = \frac{N_1 i_1(t)}{l_m}, \quad \frac{\mathrm{d}B(t)}{\mathrm{d}t} = \frac{u_2(t)}{N_2 A_m}, \tag{5}$$

where: N_1 and N_2 are the number of turns of the primary (magnetizing) and secondary (measuring) windings, respectively, l_m is the average magnetic path length of the core, A_m is the cross-sectional area of the core, i_1 is the primary winding current, u_2 is the voltage induced in the measuring winding. Taking into account Eqs. (4) and (5), the following expression can be obtained [29]:

$$P_v = \frac{1}{l_m A_m}\frac{N_1}{N_2}\frac{1}{T}\int_0^T u_2(t) i_1(t)\mathrm{d}t. \tag{6}$$

Hence, if we assume that the core volume is expressed by the product $l_m A_m$, and the number of turns of the primary and secondary windings are equal ($N_1 = N_2$), then the result of the losses P_m measured by the power analyzer, which are the product of the primary winding current i_1 and the secondary winding voltage u_2, is directly the value of the power losses in the core P_c, which is given by the relationship [29]:

This paper has been accepted for publication in the AEE journal. This is the version, which has not been fully edited and content may change prior to final publication.
Citation information: DOI 10.24425/aee.2026.3549

$$P_c = P_v l_m A_m = \frac{N_1}{N_2} P_m. \tag{7}$$

Taking into account that both measuring and magnetizing windings have the same number of turns and that these are loaded with high impedance measuring device inputs, relationships (6) and (7) can also be applied to winding N_3.

The tested core was made from ferrite magnetic material N87. The primary winding was made of litz wire 10 × 0.355 mm (number of turns $N_1 = 8$) and the measuring winding was prepared from double isolated solid wire $\phi = 0.4$ mm (number of turns $N_2 = N_3 = 8$). The main parameters of the selected ferrite core (model B64290L0647X087), based on the manufacturer data [30], are presented in Table 2.

Table 2. Selected parameters of the tested magnetic core

Core material	Core shape	μ_i	B_{sat}	l_m	A_m	V_m
			T	mm	mm^2	mm^3
Ferrite N87	ring	2 200	0.49	73.78	76.98	5 680

The second part of the measurements, containing results corresponding to the left-hand side of Eq. (1), i.e. the energy lost in the magnetic core under operating conditions of the power electronics converter, was carried out using the Brockhaus MPG-200 measurement system, which enables shaping the magnetic flux waveform in the core. The experimental setup depicted in Fig. 4.

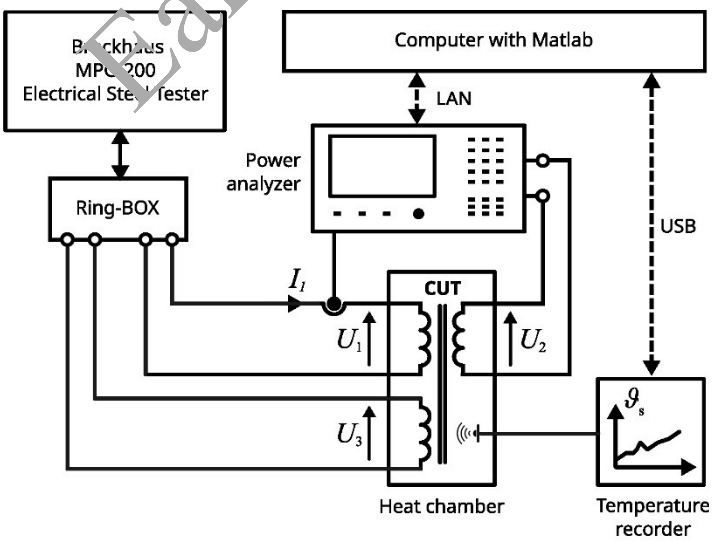

Fig. 4. Experimental measurement setup for DC-DC converter conditions

This paper has been accepted for publication in the AEE journal. This is the version, which has not been fully edited and content may change prior to final publication.
Citation information: DOI 10.24425/aee.2026.3549

In the case of measurements performed under DC–DC converter operating conditions (taking into account the assumptions presented in the previous chapter), the third winding enabled independent tracking of the shaped voltage induced by the dedicated Brockhaus MPG-200 measuring system. Although ferrite core magnetic components commonly used in power electronics DC–DC converters typically operate at frequencies of several tens of kilohertz or higher, the limitations of the custom designed power amplifier used in the setup shown in Fig. 3, together with the restricted bandwidth of the internal power amplifier of the Brockhaus MPG-200 electrical steel testing system, constrained the maximum excitation frequency to $f_{\text{rect}} = 5$ kHz, and all measurements were performed at this value. The conducted research did not consider the influence of the DC bias of the magnetic field strength on core losses. This aspect was presented only to a limited extent in [23]. For all measurements in this study, a set-point value of $H_{\text{DC}} = 0$ A/m was assumed. All measurements were performed at a forced magnetic flux density amplitude in the core of $B_m = 0.1$ T, which results from the limitations of the maximum supply voltage value of the power amplifier (the system shown in Fig. 3) and the adopted frequency conditions.

4. Estimation method

Both for measurements performed under conditions of equivalent sinusoidal excitation (Fig. 3) and those carried out using the Brockhaus MPG-200 system (Fig. 4), the Hioki PW8001 power analyzer was used to measure core losses, selected due to its high accuracy, distinguishing it from other devices of this type currently available on the market. The manufacturer of the power analyzer provides detailed information in its documentation regarding the maximum permissible errors for current, voltage, and phase-shift angle measurements across specific frequency ranges of the measured signals. It should be noted that the catalog data provided by the manufacturer refer to sinusoidal conditions. During the uncertainty estimation stage, it was also necessary to account for the additional uncertainty contribution of the Hioki CT6872 current probe used in the measurement setup. Given the magnetic flux density amplitude $B_m = 0.1$ T, which is below the saturation level B_{sat}, a simplifying assumption was made that the magnetizing current could be treated as approximately sinusoidal. Following the conservative approach recommended in the materials supplied by the power analyzer manufacturer, the value of the maximum permissible error was determined according to the following relation:

$$\Delta P_{sin} = \Delta P_{U2} + \Delta P_{I1} + \Delta P_{\phi}, \tag{8}$$

where $\Delta P_{U2}, \Delta P_{I1}, \Delta P_{\phi}$ are the components of the maximum permissible power-measurement error expressed in watts, resulting, respectively, from the measurement errors of the induced voltage U_2, the magnetizing current I_1, and the phase shift φ.

Due to the complexity and time-consuming nature of the measurement procedure, including the inertia of the thermal chamber and the absence of forced air circulation, measurement series were not performed; instead, only single measurements were carried out. Consequently, the full standard uncertainty, which would require estimating type-A uncertainty, was not determined. It was assumed that no correlation exists between the measurements of voltage, current, and phase-shift angle.

Considering the general form of the instantaneous power equation under sinusoidal conditions, as well as the defined components of the maximum permissible error in Eq. (8), the combined uncertainty of the measured power losses was estimated in accordance with [31], using the following relation:

$$u_c P_{sin} = \sqrt{u_B(U_2)^2 + u_B(I_1)^2 + u_B(\varphi)^2}, \tag{9}$$

where: P_{sin} is the power losses in watts (under sinusoidal condition), I_1 is the effective current of primary winding, U_2 is the effective voltage induced in the measuring winding, φ is the phase-shift angle between the measured voltage and current. The individual components of the type-B uncertainty, were obtained based on the known maximum permissible errors, assuming a rectangular distribution.

In the case of measurements performed under DC-DC converter operating conditions (Fig. 4), the induced voltage U_2 shaped by the Brockhaus MPG-200 system had a rectangular waveform, whereas the magnetizing current waveform was approximately triangular. Both signals are therefore non-sinusoidal, and in particular such a voltage waveform contains a large number of harmonics with significant amplitudes. Estimating losses under these conditions is a complex metrological problem. For the purpose of determining uncertainty in non-sinusoidal conditions, the procedure presented in [32] was applied, where the final general form of the combined uncertainty is expressed as follows:

$$u_c(P) = u_c(P_0) + \sum_{h=1}^{N} |u_c(P_h)|, \tag{10}$$

where: P is the power loss in watts, P_0 is the power loss associated with the DC component, P_h is the power loss for the h-th harmonic. The method for determining the uncertainty for each considered harmonic power component P_h was described in [32].

In both cases, a simplifying assumption was made that the phase-shift error compensation function (the unique ACSC function provided by Hioki) operates ideally and fully compensates for this error.

Ensuring exactly the same core temperatures, considering the accuracy and resolution of the pyrometric probe as well as the temperature-control accuracy of the thermal chamber, is very difficult in practical implementation. Therefore, in order to legitimately compare the obtained core-loss measurement results, which did not always correspond to identical temperatures, both under equivalent sinusoidal excitation and under DC-DC converter operating conditions, it was necessary to construct models of the relationship $P_V = f(\vartheta_s)$ for selected duty cycle values. In this work, the following quadratic model was adopted:

$$\hat{P}_V(\vartheta_s) = a\vartheta_s^2 + b\vartheta_s + c. \tag{11}$$

This paper has been accepted for publication in the AEE journal. This is the version, which has not been fully edited and content may change prior to final publication.
Citation information: DOI 10.24425/aee.2026.3549

Due to the presence of different uncertainty values for both the measured power losses and the temperatures, the standard approximation libraries and functions built into MATLAB were considered insufficient. Therefore, to obtain models of the highest possible accuracy, the ODRPACK95 package [33] was used, employing an open implementation of the ODR (orthogonal distance regression) algorithm [34].

The measured loss results were shifted to the desired temperature based on the obtained loss models, including the associated uncertainties. The correction of the power loss values when shifting the measured core loss values $P_{V\,\mathrm{rect}}$ or $P_{V\mathrm{eq1}}$ and $P_{V\mathrm{eq2}}$, measured at their corresponding core surface temperatures ϑ_s, to the reference temperature ϑ_{ref}, was defined as the difference between the model values:

$$\Delta P = \hat{P}_{V\mathrm{ref}}(\vartheta_{\mathrm{ref}}) - \hat{P}_{V}(\vartheta_s) = a(\vartheta_{\mathrm{ref}}^2 - \vartheta_s^2) + b(\vartheta_{\mathrm{ref}} - \vartheta_s). \tag{12}$$

In that case, the calculation of the corrected power loss value for each measurement point was performed using the following formula:

$$P_{V\mathrm{ref}} = P_V + \Delta P. \tag{13}$$

The propagation of uncertainty was performed by considering independent contributions of variance:

$$u_c^2(P_{V\mathrm{ref}}) = u_c^2(P_V) + u_\beta^2(P_V) + u_\vartheta^2(P_V), \tag{14}$$

where $u_\beta^2(P_V)$ is the variance contribution of the result $P_{V\mathrm{ref}}$ arising from the uncertainty of the estimated model parameters $\beta = [a, b, c]^T$, $u_\vartheta^2(P_V)$ is the variance contribution of the result $P_{V\,\mathrm{ref}}$ originating from the uncertainty of the temperature measurement ϑ_s.

In order to compare the results of both sides of Eq. (1), the results obtained using a self-designed measuring system (see Fig. 3) were converted into energy losses according to the formulas:

$$Q_{\mathrm{eq1}}(\Delta B, f_{\mathrm{eq1}}, \vartheta_s) = \frac{P_{\mathrm{eq1}}(\Delta B, f_{\mathrm{eq1}}, \vartheta_s)}{f_{\mathrm{eq1}}},\quad Q_{\mathrm{eq2}}(\Delta B, f_{\mathrm{eq2}}, \vartheta_s) = \frac{P_{\mathrm{eq2}}(\Delta B, f_{\mathrm{eq2}}, \vartheta_s)}{f_{\mathrm{eq2}}}. \tag{15}$$

The total energy loss under equivalent sinusoidal excitation $Q_{V\mathrm{eq\text{-}ref}}$, which corresponds to the right-hand side of Eq. (1), is the average of the sum of the components defined by Formulas (15). For the purpose of estimating the uncertainty of the determined energy loss $Q_{V\mathrm{eq\text{-}ref}}$, and due to the lack of information regarding correlation between the measurement results of the individual loss components from Eq. (15), a conservative method of estimating the uncertainty of the final result was adopted, expressed by the formula:

$$u_c(Q_{V\mathrm{eq\text{-}ref}}) = \frac{1}{2}\left[u_c(Q_{V\mathrm{eq1}}) + u_c(Q_{V\mathrm{eq2}})\right], \tag{16}$$

where the individual components of the combined uncertainties of the lost energy results $Q_{V\mathrm{eq1}}$ and $Q_{V\mathrm{eq2}}$ are identical to the uncertainties of the power measurement results $P_{V\mathrm{eq1}}$ and $P_{V\mathrm{eq2}}$. This assumption was adopted due to the high accuracy of frequency measurement provided by the Hioki analyzer (maximum permissible error $\Delta f = \pm 0.05\%$). Therefore, in all estimations performed in this work, the influence of frequency measurement uncertainty during the conversion between power losses and energy losses was omitted.

$$P_{V\text{rect-ref}}(\Delta B, f_{\text{rect}}, \vartheta_{\text{ref}}) = \overbrace{f_{\text{rect}} Q_{V\text{eq-ref}}}^{P_{V\text{eq-ref}}}(\Delta B, f_{\text{eq1}}, f_{\text{eq2}}, \vartheta_{\text{ref}}). \tag{17}$$

The reference values used to determine the accuracy of the validated method were the loss results obtained under operating conditions of the core in a DC–DC converter, measured using the setup shown in Fig. 4. The deviation of the validated method was expressed by the following equation:

$$\delta = 100\left|\frac{P_{V\text{eq-ref}} - P_{V\text{rect-ref}}}{P_{V\text{rect-ref}}}\right|. \tag{18}$$

To facilitate the analysis, the obtained results are presented in the form of power losses related to the volume of the magnetic core and are presented in the next chapter.

5. Results and Analysis

The basic results from the system shown in Fig. 3, which should be analyzed first, were the induced voltage waveforms. The following analysis concerns signal samples recorded under the most demanding operating conditions of the power amplifier, resulting from the adopted frequency range of the core operation. An exemplary induced voltage waveform $u_2(t)$, recorded by the power analyzer, together with the corresponding magnetic flux density waveform $B(t)$, are presented in Fig. 5.

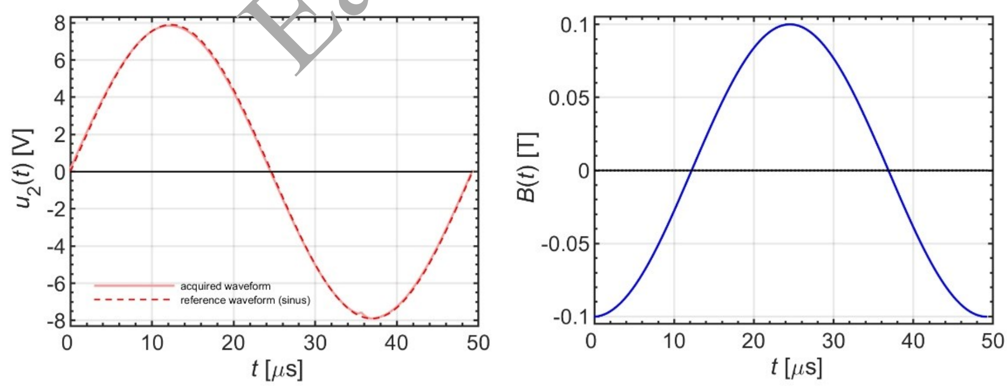

(a) (b)

Fig. 5. The obtained waveforms in the measurement setup for equivalent sinusoidal excitation at $D = 0.9$, $B_m = 100$ mT: induced voltage (a); magnetic flux density (b)

This paper has been accepted for publication in the AEE journal. This is the version, which has not been fully edited and content may change prior to final publication.
Citation information: DOI 10.24425/aee.2026.3549

The waveforms presented in Fig. 5 are the result of averaging over six periods. The number of periods used for averaging was determined by the maximum length of the recorded data containing raw measurement samples transmitted to the computer supervising the operation of the power analyzer. However, the analyzer built-in averaging algorithm was implemented as a moving-average procedure over 32 periods.

The loss components $P_{V\mathrm{eq}1}$ and $P_{V\mathrm{eq}2}$ appearing in Eqs. (15), according to the validated model, are measured under conditions of equivalent sinusoidal excitations. Hence, the correctness of the excitation conditions was assessed with reference to the requirements of the standard [21]. According to this standard, the conditions of a standardized sinusoidal excitation are met when the form factor of the induced voltage on the measurement winding reaches its nominal value $k_f = 1.111 \pm 1\%$. The calculated form factor of the recorded induced voltage waveform (Fig. 5(b)) is $k_f = 1.1107$, which indicates sufficiently accurate waveform reproduction.

Also important for verifying the correctness of the selected uncertainty estimation method for equivalent sinusoidal excitations was the shape of the magnetizing current waveform. An exemplary magnetizing current waveform $i_1(t)$, together with the resulting magnetic field strength waveform $H(t)$, is shown in Fig. 6.

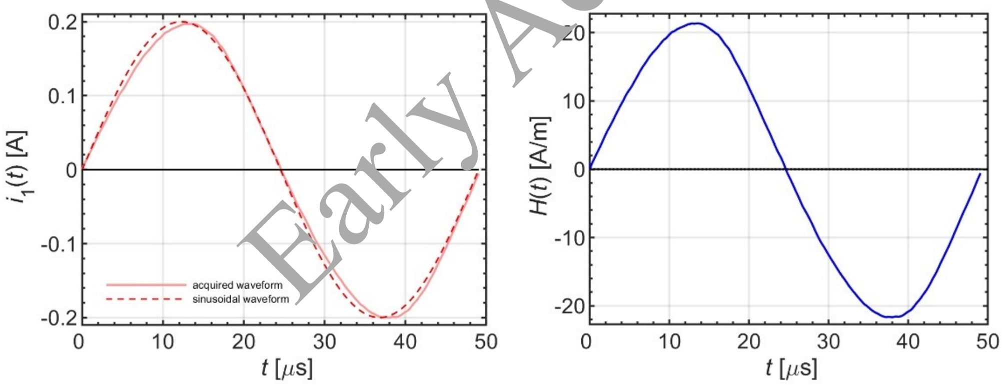

(a) (b)

Fig. 6. The obtained waveforms in the measurement setup for equivalent sinusoidal excitation at $D = 0.9$, $B_m = 100$ mT: magnetizing current (a); magnetic field strength (b)

Since for the assumed case $B_\mathrm{m} < B_\mathrm{sat}$ the core operates approximately within the linear region of its magnetization characteristic, the magnetizing current (Fig. 6(a)), and consequently the magnetic field strength waveform (Fig. 6(b)), were only slightly distorted from a sinusoidal shape ($k_f = 1.1144$). This confirms that, under these conditions, the method used to estimate the uncertainty of losses for sinusoidal equivalent excitations can be applied. The waveforms shown in Figs. 5 and 6 are not time-aligned with each other, as their analysis served solely to determine the form factor.

This paper has been accepted for publication in the AEE journal. This is the version, which has not been fully edited and content may change prior to final publication.
Citation information: DOI 10.24425/aee.2026.3549

The results obtained using the measurement method presented in Section 3 and the estimation procedure described in Section 4, are depicted in Table 3.

Table 3. Raw core loss measurements as a function of temperature and duty cycles

Duty cycle	**DC-DC converter operating condition**		**Sinusoidal excitation condition for f_{eq1}**		**Sinusoidal excitation condition for f_{eq2}**	
	Core surface temperature	**Core loss**	**Core surface temperature**	**Core loss**	**Core surface temperature**	**Core loss**
D	$\vartheta_{\mathrm{rect}} \pm u(\vartheta_{\mathrm{rect}})$	$P_V \pm u_c(P_V)$	$\vartheta_{\mathrm{eq1}} \pm u(\vartheta_{\mathrm{eq1}})$	$P_V \pm u_c(P_V)$	$\vartheta_{\mathrm{eq2}} \pm u(\vartheta_{\mathrm{eq2}})$	$P_V \pm u_c(P_V)$
-	°C	kW/m^3	°C	kW/m^3	°C	kW/m^3
0.5	30.0 ± 0.6	4.1 ± 0.2	30.7 ± 0.6	3.3 ± 0.2	30.2 ± 0.6	3.4 ± 0.2
	50.0 ± 0.6	2.66 ± 0.09	49.8 ± 0.6	2.26 ± 0.13	49.7 ± 0.6	2.26 ± 0.13
	69.2 ± 0.6	1.74 ± 0.04	70.3 ± 0.6	1.43 ± 0.09	70.3 ± 0.6	1.43 ± 0.09
	89.5 ± 0.6	1.11 ± 0.02	89.3 ± 0.6	0.96 ± 0.06	89.9 ± 0.6	0.95 ± 0.06
	99.8 ± 0.6	1.021 ± 0.015	100.1 ± 0.6	0.85 ± 0.05	100.2 ± 0.6	0.87 ± 0.05
	109.7 ± 0.6	1.14 ± 0.02	111.6 ± 0.6	0.93 ± 0.06	110.8 ± 0.6	0.94 ± 0.06
	120.3 ± 0.7	1.30 ± 0.02	120.7 ± 0.7	1.07 ± 0.06	118.1 ± 0.7	1.00 ± 0.06
0.6	30.0 ± 0.6	4.1 ± 0.2	30.6 ± 0.6	4.3 ± 0.2	30.2 ± 0.6	2.82 ± 0.15
	50.0 ± 0.6	2.68 ± 0.09	49.8 ± 0.6	2.9 ± 0.2	49.8 ± 0.6	1.88 ± 0.11
	69.1 ± 0.6	1.74 ± 0.04	70.3 ± 0.6	1.82 ± 0.11	70.3 ± 0.6	1.19 ± 0.07
	89.1 ± 0.6	1.14 ± 0.02	89.1 ± 0.6	1.22 ± 0.07	89.8 ± 0.6	0.79 ± 0.05
	99.9 ± 0.6	1.021 ± 0.015	100.1 ± 0.6	1.10 ± 0.07	100.1 ± 0.6	0.71 ± 0.04
	109.6 ± 0.6	1.18 ± 0.02	111.5 ± 0.6	1.20 ± 0.07	110.7 ± 0.6	0.77 ± 0.05
	120.4 ± 0.7	1.30 ± 0.02	121.0 ± 0.7	1.33 ± 0.08	118.2 ± 0.7	0.82 ± 0.05
0.7	29.9 ± 0.6	4.1 ± 0.2	30.6 ± 0.6	5.6 ± 0.3	30.3 ± 0.6	2.39 ± 0.12
	49.9 ± 0.6	2.71 ± 0.09	49.7 ± 0.6	3.8 ± 0.2	49.8 ± 0.6	1.60 ± 0.09
	69.1 ± 0.6	1.76 ± 0.04	70.2 ± 0.6	2.43 ± 0.15	70.3 ± 0.6	1.01 ± 0.06
	88.9 ± 0.6	1.14 ± 0.02	89.1 ± 0.6	1.65 ± 0.10	89.6 ± 0.6	0.67 ± 0.04
	99.9 ± 0.6	1.06 ± 0.02	100.0 ± 0.6	1.48 ± 0.09	100.1 ± 0.6	0.61 ± 0.04
	109.5 ± 0.6	1.20 ± 0.02	111.4 ± 0.6	1.6 ± 0.1	110.7 ± 0.6	0.67 ± 0.04
	120.6 ± 0.7	1.34 ± 0.02	121.2 ± 0.7	1.85 ± 0.11	118.3 ± 0.7	0.71 ± 0.04
0.8	30.0 ± 0.6	4.1 ± 0.2	30.5 ± 0.6	9 ± 1	30.3 ± 0.6	2.14 ± 0.11
	49.8 ± 0.6	2.73 ± 0.09	49.7 ± 0.6	6.0 ± 0.8	49.7 ± 0.6	1.39 ± 0.08

This paper has been accepted for publication in the AEE journal. This is the version, which has not been fully edited and content may change prior to final publication.
Citation information: DOI 10.24425/aee.2026.3549

	68.9 ± 0.6	1.80 ± 0.05	70.2 ± 0.6	3.8 ± 0.5	70.3 ± 0.6	0.86 ± 0.05
	88.6 ± 0.6	1.20 ± 0.02	89.1 ± 0.6	2.6 ± 0.4	89.5 ± 0.6	0.60 ± 0.04
	99.8 ± 0.6	1.07 ± 0.02	100.0 ± 0.6	2.4 ± 0.3	100.2 ± 0.6	0.54 ± 0.03
	109.5 ± 0.6	1.18 ± 0.02	111.3 ± 0.6	2.6 ± 0.3	110.7 ± 0.6	0.56 ± 0.03
	120.6 ± 0.7	1.37 ± 0.02	121.3 ± 0.7	2.9 ± 0.4	118.5 ± 0.7	0.63 ± 0.04
0.9	29.9 ± 0.6	4.3 ± 0.2	30.2 ± 0.6	18 ± 2	30.2 ± 0.6	1.9 ± 0.1
	49.7 ± 0.6	2.92 ± 0.11	49.6 ± 0.6	13 ± 2	49.7 ± 0.6	1.25 ± 0.07
	68.7 ± 0.6	1.90 ± 0.05	70.0 ± 0.6	8.5 ± 1.2	70.3 ± 0.6	0.79 ± 0.05
	90.0 ± 0.6	1.29 ± 0.02	89.3 ± 0.6	6.0 ± 0.8	89.4 ± 0.6	0.53 ± 0.03
	99.8 ± 0.6	1.14 ± 0.02	99.9 ± 0.6	5.4 ± 0.7	100.1 ± 0.6	0.48 ± 0.03
	109.6 ± 0.6	1.27 ± 0.02	111.2 ± 0.6	5.9 ± 0.8	110.9 ± 0.6	0.50 ± 0.03
	120.7 ± 0.7	1.50 ± 0.03	121.4 ± 0.7	6.9 ± 0.9	118.6 ± 0.7	0.55 ± 0.03

The coefficients of the quadratic model (11), expressing the dependence of the volumetric core losses on temperature (including the prior normalization to the reference temperature ϑ_{ref}), were obtained using the Orthogonal Distance Regression algorithm with the ODRPACK95 library [33] in the implementation described in [34]. The resulting coefficients are presented below in Tables 4 and 5.

Table 4. Estimated model coefficient values with standard and relative uncertainties for $P_{V\mathit{rect}\text{-ref}}$

Duty cycle	Estimated coefficients with standard and relative uncertainties					
D	$a \pm u(a)$	$u_r(a)$	$b \pm u(b)$	$u_r(b)$	$c \pm u(c)$	$u_r(c)$
-	kWm^{-3}°C^{-2}	%	kWm^{-3}°C^{-1}	%	kWm^{-3}	%
0.5	0.00067 ± 0.00004	6	–0.132 ± 0.008	6	7.6 ± 0.4	5
0.6	0.00067 ± 0.00006	9	–0.134 ± 0.011	8	7.7 ± 0.5	6
0.7	0.00067 ± 0.00005	7	–0.132 ± 0.009	7	7.6 ± 0.4	5
0.8	0.00065 ± 0.00004	6	–0.131 ± 0.007	5	7.6 ± 0.3	4
0.9	0.00069 ± 0.00005	7	–0.138 ± 0.009	7	8.1 ± 0.4	5

Table 5. Estimated model coefficient values with standard and relative uncertainties for $P_{V\text{eq-ref}}$

Duty cycle	Estimated coefficients with standard and relative uncertainties					
D	$a \pm u(a)$	$u_r(a)$	$b \pm u(b)$	$u_r(b)$	$c \pm u(c)$	$u_r(c)$
-	kWm^{-3}°C^{-2}	%	kWm^{-3}°C^{-1}	%	kWm^{-3}	%

0.5	0.00061 ± 0.00002	3	–0.126 ± 0.004	3	7.5 ± 0.2	3
0.6	0.00060 ± 0.00002	3	–0.125 ± 0.004	3	7.5 ± 0.2	3
0.7	0.00060 ± 0.00002	3	–0.124 ± 0.004	3	7.5 ± 0.2	3
0.8	0.000603 ± 0.000011	1.8	–0.124 ± 0.002	1.6	7.5 ± 0.08	1.1
0.9	0.00062 ± 0.00003	5	–0.127 ± 0.004	3	7.7 ± 0.2	3

It is noteworthy that the models obtained from measurements under equivalent-excitation conditions (Table 5) exhibit lower uncertainties than the models derived under DC–DC converter operating conditions (Table 4). Since these uncertainties are not clearly dependent on the duty cycle value, it can be concluded that this effect is not related to the limited bandwidth of the Brockhaus MPG-200 power-amplifier system, whose bandwidth limitations would be more pronounced at extreme duty cycle values ($D = 0.9$ in the considered range). The analysis of the estimated uncertainties indicates that the relationship $P_V = f(\vartheta)$ expressed by the quadratic model for the investigated ferrite, is better satisfied by the measurement results corresponding to the right-hand side of the validated Eq. (1).

The plots showing the volumetric power losses P_{Veq1} and P_{Veq2} obtained for the most extreme duty cycle value ($D = 0.9$), under equivalent sinusoidal excitation at frequencies f_{eq1} and f_{eq2}, respectively, are presented in Fig. 7. As can be observed, their loss levels differ significantly, since according to Eq. (2) the frequencies $f_{eq1}(D = 0.9) \approx 20\,264$ Hz and $f_{eq2}(D = 0.9) \approx 2\,252$ Hz differ by an order of magnitude. According to the theory presented in [35], in the case where $f_{eq2} < f_{eq1}$, the decrease in frequency results in a corresponding reduction in losses, assuming that all other operating conditions of the magnetic core remain unchanged. The raw measurement results (Table 3) obtained under the same conditions for the case of $D = 0.5$ are nearly identical, since in this situation the equivalent frequencies resulting from Eq. (2) are the same.

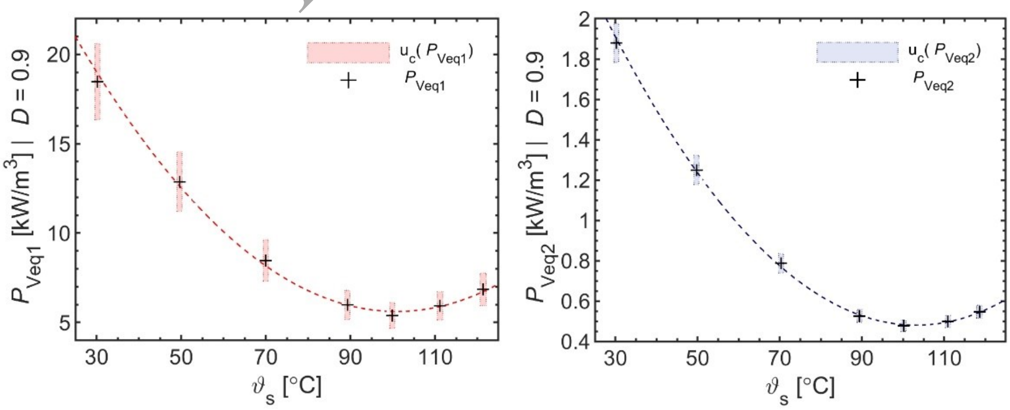

(a) (b)

Fig. 7. Raw core losses measured at frequencies f_{eq1} (a) and f_{eq2} (b) for duty cycle $D = 0.9$

This paper has been accepted for publication in the AEE journal. This is the version, which has not been fully edited and content may change prior to final publication.
Citation information: DOI 10.24425/aee.2026.3549

A comparison of the final values of $P_{V\,\mathrm{rect\text{-}ref}}$ and $P_{V\mathrm{eq\text{-}ref}}$, estimated after shifting to the reference temperatures according to the procedure presented in the previous section, is depicted for the case $D = 0.9$ in Fig. 8.

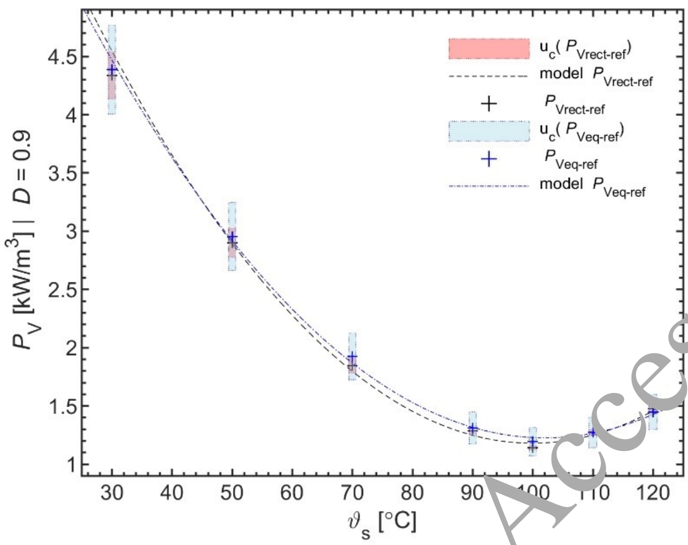

Fig. 8. Comparison of core loss results normalized to reference temperatures for sinusoidal excitation and under DC–DC converter operating conditions

The estimated loss results (Fig. 8) correspond exactly to the values of the reference temperatures. As can be observed, the losses corresponding to both sides of Eq. (17) are largely consistent, and the uncertainties of the losses measured under sinusoidal excitation conditions have higher values. The main reason for this is the fact that the first component of the dissipated energy Q_{eq1} was always measured, within the adopted duty cycle range (except for the symmetric rectangular wave case $D = 0.5$), at equivalent frequencies f_{eq1} higher than the frequency of the waveform under f_{rect} conditions. The noticeable differences in uncertainty (Fig. 8) are expected, since the accuracy of the power analyzer decreases with increasing signal frequency, and also due to the differences in the approach to loss estimation depending on whether the waveform is sinusoidal or strongly distorted. A second factor is that the components Q_{eq1} and Q_{eq2}, according to Eq. (1), are added together with their uncertainties accounted for according to the methodology presented in the previous section.

The results indicate that the optimal operating temperature of the tested ferrite core is about 100°C, at which the core loss level is the lowest. This is consistent with the technical data provided by the core manufacturer. However, it should be noted that some ferrite materials exhibit only a small change in losses with core temperature, e.g., N95 ferrite.

From the perspective of a DC-DC power converter designer, characteristics showing the dependence $P_V = f(D)$ provide essential information about magnetic core losses. Based on the conducted measurements, the estimated loss results as a function of duty cycle for various temperatures are depicted in Fig. 9.

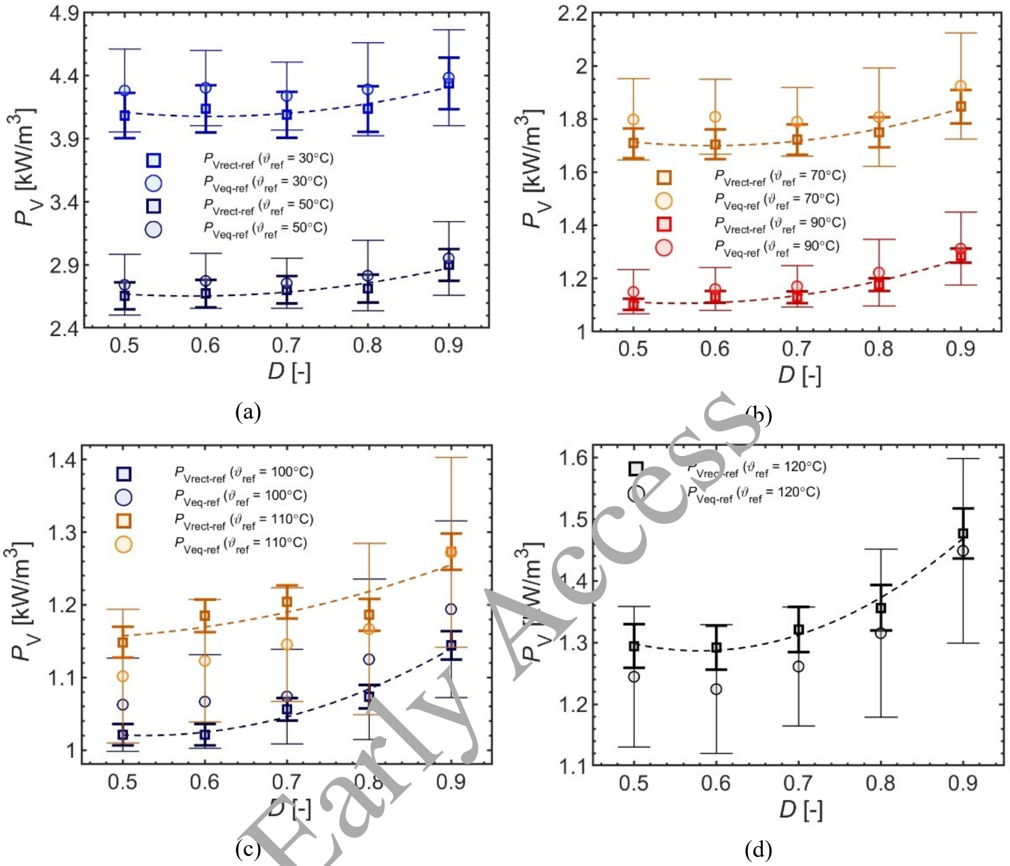

Fig. 9. Core loss results as a function of duty cycle for different reference temperatures: for 30°C and 50°C (a); for 70°C and 90°C (b); for 100°C and 110°C (c); and for 120°C (d)

Modeling of loss phenomena in the magnetic core operating in DC-DC power converters, taking into account the wide variation in duty cycle values, has been the subject of numerous studies, e.g. [1, 5, 36]. These relationships are shown in Fig. 9, where the dashed line represents an approximation of the $P_{V\,\mathrm{rect\text{-}ref}}$ results. In these plots, the dashed line marks the approximation of the $P_{V\,\mathrm{rect\text{-}ref}}$ results. Since the inaccuracy of duty cycle measurement was omitted, the approximation was performed using the built-in MATLAB function *nlinfit*. Analyzing the core-loss results as a function of duty cycle, presented in the form of plots including the estimated uncertainties (Fig. 9), it can be observed that in most cases the results corresponding to both sides of Eq. (17) are consistent with each other. It can also be noted that the core losses generally increase with increasing duty cycle under all temperature conditions (more precisely, with increasing deviation from $D = 0.5$, since the dependence $P_V = f(\vartheta)$ is symmetric with respect to this duty cycle value).

This paper has been accepted for publication in the AEE journal. This is the version, which has not been fully edited and content may change prior to final publication.
Citation information: DOI 10.24425/aee.2026.3549

A summary of the final volumetric core loss estimates together with their uncertainties, including the calculated deviation of the validated method, for selected core surface temperatures and duty cycle values, is presented in Table 6. Due to the fact that in some cases the estimated deviations of the method turned out to be relatively low and close to one another, these values were intentionally presented with one decimal place. The deviation itself, however, was evaluated on the basis of the precise estimated loss values, of which only the rounded results, in accordance with [31], are presented in Table 6.

Analyzing the obtained results, it can be observed that the highest value of the estimated deviation of the method reached 6%, while in most points it remained below 5%. This indicates that the validated method exhibits good convergence. The uncertainties of the estimated core losses under equivalent sinusoidal excitation conditions, shifted to the reference temperatures, were generally comparable to or greater than the uncertainties of the losses estimated under DC-DC converter operating conditions (also shifted to the reference temperatures). This is an expected outcome due to the generally higher uncertainties of the raw loss measurements (Table 3) and the need to further sum individual components according to (16).

Equation (17), for the case of power-loss considerations and thus the original Eq. (1) presented in [23] for lost energy considerations describes with satisfactory accuracy and under the adopted simplifying assumptions, the losses corresponding to the operation of a magnetic core in a DC-DC power converter.

A detailed analysis of the results summarized in Fig. 9 and Table 6 shows that in some cases the minimum loss was not observed exactly at $D = 0.5$. These deviations from theory, although small, are noticeable and could be further verified by performing an extended series of measurements. However, such measurements would require significantly more effort due to the thermal inertia of both the used temperature chamber and the core itself. Therefore, in this type of experiment, a temperature chamber with better dynamic performance (forced-air circulation) and a smaller core would be preferable, although the latter is limited by the need to ensure a sufficiently large observable surface area for the pyrometric sensor.

Table 6. Summary of the final estimates of the core losses, including the evaluated deviation of the validated method, for selected temperatures and duty cycle values

Duty cycle	**Reference core surface temperature**	**DC-DC converter operating condition**	**Sinusoidal excitation condition**	**Method deviation**
D	ϑ_{ref}	$P_{V\,\text{rect-ref}} \pm u_c(P_{V\,\text{rect-ref}})$	$P_{V\text{eq-ref}} \pm u_c(P_{V\text{eq-ref}})$	δ
-	°C	kW/m^3	kW/m3	%
0.5	30	4.1 ± 0.2	4.3 ± 0.3	4.9
	50	2.66 ± 0.11	2.7 ± 0.2	3.2
	70	1.71 ± 0.06	1.8 ± 0.2	5.2
	90	1.10 ± 0.02	1.15 ± 0.08	4.3
	100	1.021 ± 0.015	1.06 ± 0.06	4.1

This paper has been accepted for publication in the AEE journal. This is the version, which has not been fully edited and content may change prior to final publication.
Citation information: DOI 10.24425/aee.2026.3549

	110	1.15 ± 0.02	1.10 ± 0.09	4.1
	120	1.29 ± 0.04	1.24 ± 0.11	3.9
0.6	30	4.1 ± 0.2	4.3 ± 0.3	4.0
	50	2.68 ± 0.11	2.8 ± 0.2	3.7
	70	1.71 ± 0.06	1.81 ± 0.14	6.0
	90	1.13 ± 0.02	1.16 ± 0.08	2.5
	100	1.021 ± 0.015	1.07 ± 0.06	4.5
	110	1.19 ± 0.02	1.12 ± 0.08	5.2
	120	1.29 ± 0.04	1.22 ± 0.10	5.2
0.7	30	4.1 ± 0.2	4.2 ± 0.3	3.6
	50	2.70 ± 0.11	2.8 ± 0.2	2.0
	70	1.72 ± 0.06	1.79 ± 0.13	3.9
	90	1.13 ± 0.02	1.17 ± 0.08	3.7
	100	1.06 ± 0.02	1.07 ± 0.07	1.6
	110	1.20 ± 0.02	1.15 ± 0.08	4.9
	120	1.32 ± 0.04	1.3 ± 0.1	4.5
0.8	30	4.1 ± 0.2	4.3 ± 0.4	3.8
	50	2.72 ± 0.11	2.8 ± 0.3	3.7
	70	1.75 ± 0.06	1.8 ± 0.2	3.3
	90	1.18 ± 0.02	1.22 ± 0.12	3.8
	100	1.07 ± 0.02	1.12 ± 0.11	4.8
	110	1.19 ± 0.02	1.17 ± 0.12	1.7
	120	1.36 ± 0.04	1.32 ± 0.14	3.0
0.9	30	4.3 ± 0.2	4.4 ± 0.4	1.1
	50	2.90 ± 0.12	3.0 ± 0.3	1.8
	70	1.85 ± 0.06	1.9 ± 0.2	4.2
	90	1.29 ± 0.03	1.31 ± 0.14	2.1
	100	1.14 ± 0.02	1.19 ± 0.12	4.3
	110	1.27 ± 0.03	1.27 ± 0.13	0.1
	120	1.48 ± 0.04	1.45 ± 0.15	1.9

This paper has been accepted for publication in the AEE journal. This is the version, which has not been fully edited and content may change prior to final publication.
Citation information: DOI 10.24425/aee.2026.3549

6. Conclusion

The presented research focused on verification of a known magnetic core loss prediction method based on sinusoidal loss data. This method was validated for various duty cycle values and core surface temperatures, which constituted the original research contribution of this work. For the purpose of the experimental verification, a measurement setup for sinusoidal excitation was constructed, and the results were compared with those obtained using a dedicated measurement system that allowed the reproduction of triangular magnetic flux density waveforms in the tested core. A procedure for estimating measurement uncertainties and converting them to selected reference temperatures was developed to ensure a reliable quantitative assessment of the method.

On the basis of the obtained measurement results and the conducted analyses, it can be concluded that the validated method is suitable for predicting core losses under triangular magnetic flux density waveforms using losses measured under sinusoidal excitation, within the adopted measurement conditions and assumptions. The selected range of measured core surface temperatures allowed identifying the minimum operating point of the tested N87 ferrite core. However, due to hardware limitations, the good convergence of the method was confirmed only for relatively low frequencies corresponding to $f_{\mathrm{rect}} = 5$ kHz, which is a low operating frequency for this type of core. Therefore, extending the investigation to higher frequencies is recommended, which requires appropriate modifications to the presented experimental setups.

The observed increase in core losses as a function of duty cycle variation was not significantly large. The temperature of the core had a much stronger influence on the losses of the tested material. From the perspective of designing magnetic components for DC-DC converters, determining these increments at higher frequencies and for other values of maximum magnetic flux density than $B_m = 0.1$ T may be particularly valuable. It is also advisable to perform a series of measurements, which requires the use of a temperature chamber with sufficiently good dynamic performance. Such extensive measurements, while maintaining appropriate rigor in the quantitative assessment of results, may constitute an interesting subject for further research.

References

[1] Barg S., Ammous K., Mejbri H., Ammous A., *An improved empirical formulation for magnetic core losses estimation under nonsinusoidal induction*, IEEE Transactions on Power Electronics, vol. 32, no. 3, pp. 2146–2154 (2017), DOI: 10.1109/TPEL.2016.2555359.

[2] Fortune Business Insights Pvt. Ltd., *Switch mode power supply market size, share, and industry analysis by type (AC to DC, DC to DC, and others), by end user (consumer electronics, industrial, communication, data centers, and others), and regional forecast, 2026-2034*, https://www.fortunebusinessinsights.com/switch-mode-power-supply-market-111021, accessed July 2026.

[3] Rodriguez-Sotelo D., Rodriguez-Licea M., Soriano-Sanchez A., Espinosa-Calderon A., Perez-Pinal F., *Advanced ferromagnetic materials in power electronic converters: A state of the art*, IEEE Access, vol. 8, pp. 56238–56252 (2020), DOI: 10.1109/ACCESS.2020.2982161.
[4] Reusch D., Strydom J., Glaser J., *Improving high frequency DC-DC converter performance with monolithic half bridge GaN ICs*, Proceedings of 7th IEEE Energy Conversion Congress and Exposition, Montreal, Canada, pp. 381–387 (2015), DOI: 10.1109/ECCE.2015.7309713.
[5] Li Z., Han W., Xin Z., Liu Q., Chen J., Loh P., *A review of magnetic core materials, core loss modeling and measurements in high-power high-frequency transformers*, CPSS Transactions on Power Electronics and Applications, vol. 7, no. 4, pp. 359–373 (2022), DOI: 10.24295/CPSSTPEA.2022.00033.
[6] Grzejszczak P., Barlik R., Wolski K., *Analysis and estimation of power losses in high-power, high-frequency transformers for isolated DC/DC converters*, Archives of Electrical Engineering, vol. 73, no. 3, pp. 817–830 (2024), DOI: 10.24425/aee.2024.150897.
[7] Van Dijk E., Spruijt J., O'Sullivan D., Klaassens J., *PWM-switch modeling of DC-DC converters*, IEEE Transactions on Power Electronics, vol. 10, no. 6, pp. 659–665 (1995), DOI: 10.1109/63.471285.
[8] Bryant B., Kazimierczuk M., *Modeling the closed-current loop of PWM boost DC-DC converters operating in CCM with peak current-mode control*, IEEE Transactions on Circuits and Systems I: Regular Papers, vol. 52, no. 11, pp. 2404–2412 (2005), DOI: 10.1109/TCSI.2005.853904.
[9] Janke W., *Small-signal transmittances of DC-DC step-down PWM converter in various operation modes*, Archives of Electrical Engineering, vol. 64, no. 3, pp. 505–529 (2015), DOI: 10.2478/aee-2015-0038.
[10] Dutta S., Bhattacharya S., *A method to measure the DC bias in high frequency isolation transformer of the dual active bridge DC to DC converter and its removal using current injection and PWM switching*, Proceedings of 6th IEEE Energy Conversion Congress and Exposition, Pittsburgh, United States of America, pp. 1134–1139 (2014), DOI: 10.1109/ECCE.2014.6953527.
[11] Kazimierczuk M., *Pulse-width modulated DC-DC power converters*, John Wiley & Sons (2015), DOI: 10.1002/9781119009597.
[12] Barlik R., Nowak M., *Energoelektronika – elementy, podzespoły, układy*, Oficyna Wydawnicza Politechniki Warszawskiej (2014).
[13] Brockmeyer A., *Experimental evaluation of the influence of DC-premagnetization on the properties of power electronic ferrites*, in Applied Power Electronics Conference and Exposition (APEC), © APEC (1996), DOI: 10.1109/APEC.1996.500481.
[14] Mühlethaler J., Biela J., Kolar J., Ecklebe A., *Core losses under the DC bias condition based on Steinmetz parameters*, in International Power Engineering Conference (IPEC), © IPEC (2010), DOI: 10.1109/IPEC.2010.5542385.
[15] Sun H., Li Y., Lin Z., Zhang C., Yue S., *Core loss separation model under square voltage considering DC bias excitation*, AIP Advances, vol. 10, no. 1, pp. 1–6, 015229 (2020), DOI: 10.1063/1.5131561.
[16] Olivier C., *A new core loss model*, Switching Power Magazine, pp. 1–3 (2002).
[17] Gzieł D., Najgebauer M., *Review of power loss models for magnetic cores operating in power electronic systems*, Przegląd Elektrotechniczny (in Polish), vol. 96, no. 12, pp. 238–242 (2020), DOI: 010.15199/48.2020.12.52.
[18] Yue S., Li Y., Yang Q., Yu X., Zhang C., *Comparative analysis of core loss calculation methods for magnetic materials under nonsinusoidal excitations*, IEEE Transactions on Magnetics, vol. 54, no. 11 (2018), DOI: 10.1109/TMAG.2018.2842064.
[19] Gzieł D., Jąderko A., Pawlikowski T., *Experimental verification of the simplified modeling of inductor losses operating in a DC/DC converter using the Matlab-Simulink program*, Przegląd Elektrotechniczny (in Polish), no. 3, pp. 44–48 (2025), DOI: 10.15199/48.2025.03.11.
[20] Tumanski S., *Handbook of magnetic measurements*, CRC Press (2016), DOI: 10.1201/b10979.
[21] PKN, *Magnetic materials – Part 6: Methods of measurement of AC magnetic properties of soft magnetic materials*, PN-EN IEC 60404-6 (2018).

This paper has been accepted for publication in the AEE journal. This is the version, which has not been fully edited and content may change prior to final publication.
Citation information: DOI 10.24425/aee.2026.3549

[22] Albach M., Duerbaum T., Brockmeyer A., *Calculating core losses in transformers for arbitrary magnetizing currents, a comparison of different approaches*, in Power Electronics Specialists Conference (PESC), © PESC (1996), DOI: 10.1109/PESC.1996.548774.
[23] Matsumori H., Shimizu T., Kosaka T., Matsui N., *Core loss calculation for power electronics converter excitation from a sinusoidal excited core loss data*, AIP Advances, vol. 10, no. 4, pp. 1–4, 045001 (2020), DOI: 10.1063/1.5129419.
[24] Yamashita Y., Furuta J., Inamori S., Kobayashi K., *Design of RCD snubber considering wiring inductance for MHz-switching of SiC-MOSFET*, Proceedings of IEEE 18th Workshop on Computers in Power Electronics (COMPEL), Stanford, United States of America, pp. 1–6 (2017), DOI: 10.1109/COMPEL.2017.8013396.
[25] Mu M., Li Q., Gilham D., Lee F., Ngo K., *New core loss measurement method for high frequency magnetic materials*, Proceedings of 2nd IEEE Energy Conversion Congress and Exposition, Atlanta, United States of America, pp. 4384–4389 (2010), DOI: 10.1109/ECCE.2010.5618454.
[26] Kyaw A., Delhommais M., Qiu J., Sullivan C., Schanen J., Rigaud C., *Thermal modeling of inductor and transformer windings including litz wire*, IEEE Transactions on Power Electronics, vol. 35, no. 1, pp. 867–881 (2020), DOI: 10.1109/TPEL.2019.2914661.
[27] McLyman T., *Transformer and inductor design handbook*, CRC Press (2017), DOI: 10.1201/b10865.
[28] TDK Electronics, *Ferrites and accessories, SIFERRIT material N87*, datasheet, https://www.tdk-electronics.tdk.com/en/529404/products/product-catalog/ferrites-and-accessories/ferrite-materials, accessed July 2026.
[29] Hayashi K., *Measurement of loss in high-frequency reactors*, Hioki (2016).
[30] TDK Electronics, *Ferrites and accessories, Toroids (ring cores) R29.5x19.0x14.9*, datasheet, https://product.tdk.com/en/search/ferrite/ferrite/ferrite-core/info?part_no=B64290L0647X087, accessed July 2026.
[31] JCGM, *Evaluation of measurement data — Guide to the expression of uncertainty in measurement*, JCGM 100:2008 (2008).
[32] Demerdziev K., Dimchev V., *Active power measurement uncertainty modelling and propagation analysis in case of harmonically distorted signals*, Acta IMEKO, vol. 12, no. 3, pp. 1–10 (2023), DOI: 10.21014/actaimeko.v12i3.1463.
[33] Zwolak J., Boggs P., Watson L., *Algorithm 869: ODRPACK95: A weighted orthogonal distance regression code with bound constraints*, ACM Transactions on Mathematical Software, vol. 33, no. 4 (2007), DOI: 10.1145/1268776.1268782.
[34] Vale H., *ODRPACK: Python bindings for ODRPACK95 (v0.6.1)*, https://github.com/HugoMVale/odrpack-python, accessed July 2026.
[35] Steinmetz C., *On the law of hysteresis*, Transactions of the American Institute of Electrical Engineers, vol. 9, pp. 3–64 (1892).
[36] Guillod T., Lee J., Li H., Wang S., Chen M., Sullivan C., *Calculation of Ferrite Core Losses with Arbitrary Waveforms using the Composite Waveform Hypothesis*, in IEEE Applied Power Electronics Conference and Exposition (APEC), © APEC (2023), DOI: 10.1109/APEC43580.2023.10131348.